Letter

Benjamin J. Roman and Matthew T. Sheldon*

Six-fold plasmonic enhancement of thermal scavenging via $CsPbBr_3$ anti-Stokes photoluminescence

https://doi.org/10.1515/nanoph-2018-0196
Received November 16, 2018; revised January 7, 2019; accepted January 15, 2019

Abstract: One-photon up-conversion, also called anti-Stokes photoluminescence (ASPL), is the process whereby photoexcited carriers scavenge thermal energy and are promoted into a higher energy excited state before emitting a photon of greater energy than initially absorbed. Here, we examine how ASPL from $CsPbBr_3$ nanoparticles is modified by coupling with plasmonically active gold nanoparticles deposited on a substrate. Two coupling regimes are examined using confocal fluorescence microscopy: three to four Au nanoparticles per diffraction limited region and monolayer Au nanoparticle coverage of the substrate. In both regimes, $CsPbBr_3$ ASPL is blue-shifted relative to $CsPbBr_3$ deposited on a bare substrate, corresponding to an increase in the thermal energy scavenged per emitted photon. However, with monolayer Au nanoparticle coverage, ASPL is enhanced relative to the conventional Stokes-shifted PL. Together, these phenomena result in a 6.7-fold increase in the amount of thermal energy extracted from the system during optical absorption and reemission.

Keywords: optical cooling; plasmon; perovskite; up-conversion; anti-Stokes photoluminescence.

1 Introduction

The photoluminescence (PL) produced by semiconductors generally undergoes a Stokes shift, whereby emitted photons have lower energy than those absorbed. Often, this disparity in energy is due to thermalization losses. An excited carrier nonradiatively relaxes to an excited state with lower energy before emitting the leftover energy as a photon that is red-shifted compared to the exciton absorption. The converse process, in which a material emits higher energy light than it absorbs, is commonly known as luminescence up-conversion [1, 2]. While the majority of research into luminescence up-conversion is focused on nonlinear, multi-photon excitation mechanisms, there are material systems for which one-photon up-conversion, also called anti-Stokes photoluminescence (ASPL), is possible [3–11]. As the name implies, ASPL is the reverse process of the thermalization loss that gives rise to Stokes-shifted PL. In a system with two closely spaced excited states with an energy difference no more than a few kT, carriers excited into the lower excited state may scavenge thermal energy and be promoted into a higher excited state. The carriers then radiatively relax, emitting a photon with energy equal to the absorbed photon plus the scavenged thermal energy (Figure 1). If this ASPL occurs with high quantum yield compared to other photothermalization losses, the system will undergo optically driven cooling [3, 6, 8, 10, 11]. Such cooling has often been demonstrated in materials doped with rare-earth metals [8, 9]; however, the thermal population of their electronic state manifolds is unsuitable for cooling below 100 K [9, 10].

One of the major hurdles to overcome in order to demonstrate optical cooling is the requirement that a system must have an external quantum efficiency of 99% or higher. Otherwise, reabsorption and nonradiative decay lead to thermalization losses that are larger than the amount of thermal energy removed from the system through ASPL. Colloidal semiconducting nanoparticles represent a relatively unexplored but attractive alternative material system for optically driven cooling because of their high PL quantum efficiency, as well as favorable low temperature ground state populations that allow for optical cooling at temperatures as low as 10 K [6, 9, 10]. Surprisingly, while ASPL

***Corresponding author: Matthew T. Sheldon,** Department of Chemistry, Department of Materials Science & Engineering, Texas A&M University, College Station, TX, USA, e-mail: sheldonm@tamu.edu. https://orcid.org/0000-0002-4940-7966
Benjamin J. Roman: Department of Chemistry, Texas A&M University, College Station, TX, USA. https://orcid.org/0000-0003-2213-2533

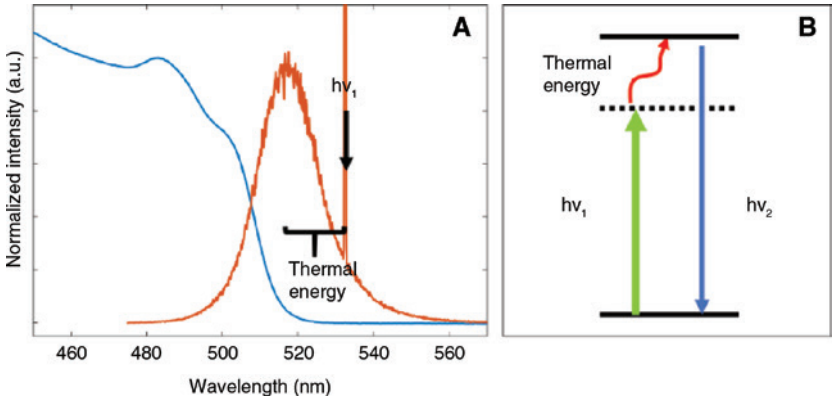

Figure 1: Illustration of anti-Stokes photoluminescence.
(A) Absorption (blue) and anti-Stokes photoluminescence (orange) of $CsPbBr_3$ nanoparticles, with the excitation wavelength marked.
(B) Schematic of the one-photon up-conversion mechanism.

appears to be rather ubiquitous in colloidal semiconductor nanoparticles [4, 6, 11–15], measurable cooling has only been demonstrated in two semiconducting systems: CdS nanobelts [4, 11] and hybrid organic-inorganic perovskite thin films [3]. The ASPL observed from colloidal nanomaterials has conventionally been thought to be due to mid-gap surface traps that act as discrete, long-lived intermediate states [4, 16]. However, very recently it was observed that all-inorganic $CsPbX_3$ (X = Cl, Br, or I) perovskite nanoparticles demonstrate ASPL with quantum efficiencies as high as 75% [5] and Stokes-shifted PL (SSPL) quantum efficiencies as high as 100% [17]. Such a high efficiency seems at odds with the need for mid-gap intermediate states, as all-inorganic perovskite nanoparticles are understood to be generally absent of mid-gap trap states [18]. In fact, we recently reported that $CsPbBr_3$ ASPL efficiency increases when essentially all mid-gap trap states are removed via a facile surface treatment [7]. Our prior results suggest that mid-gap trap states act as loss pathways rather than necessary intermediate excited states for ASPL. Rather, it is possible that the ASPL excitation mechanism proceeds through a virtual state, in a manner more analogous to anti-Stokes Raman scattering. As such, it may be feasible to increase the thermal scavenging potential of the ASPL using a plasmonically active substrate, leveraging the same light-matter interactions that can also enhance Raman scattering, as is well known for surface enhanced Raman spectroscopy (SERS) [19]. The localized surface plasmon resonance of a metal nanostructure, e.g. gold nanoparticles, enhances the optical field and increases the local-mode density of the electromagnetic field, improving the coupling efficiency of the electromagnetic excitation to vibrational modes, i.e. phonons, in the nanocrystal lattice.

Here, we report the modification of $CsPbBr_3$ ASPL through coupling to Au nanoparticles deposited on a glass substrate. Two regimes of coupling are examined using confocal fluorescence microscopy. When Au nanoparticles are limited to approximately three to four particles for every diffraction-limited region, called low coverage from hereon, the ASPL blue-shifts by as much as 7.2 meV compared with the ASPL of control samples of pure films of $CsPbBr_3$ nanoparticles without Au nanoparticles. This blue-shift corresponds to a fraction of the longitudinal optical (LO) phonon, which is known to have energy of ~20 meV in $CsPbBr_3$ nanoparticles. When $CsPbBr_3$ nanoparticles are deposited on a substrate coated in a monolayer film of densely packed Au nanoparticles, called uniform coverage from hereon, the ASPL both blue-shifts and increases in intensity relative to the SSPL measured over the same region. The blue-shift indicates a greater amount of thermal energy scavenged per emitted photon during ASPL and is likely due to a decrease in the fluorescent lifetime. In contrast, the increase in ASPL yield relative to SSPL is due to plasmonic enhancement of the intrinsic ASPL mechanism. These two effects, and the accompanying six-fold improvement in overall thermal energy scavenging, may help enable future optoelectronic applications of optical cooling and are an intriguing method of improving the ASPL performance in all-inorganic perovskite nanoparticles by coupling them with Au nanoparticle plasmons.

2 Results and discussion

In order to elucidate the interactions between $CsPbBr_3$ and gold nanoparticles, two substrates were prepared with varying amounts of 40 nm diameter gold nanoparticles deposited onto cover slips via centrifugation: one with 50 Au nanoparticles per μm^2 corresponding to

approximately three to four gold nanoparticles per diffraction limited region and one with 250 Au nanoparticles per μm^2 corresponding to a monolayer of Au nanoparticles. A clean glass cover slip was used as the control substrate. $CsPbBr_3$ nanoparticles were drop-cast onto these substrates by depositing a 1 µl drop of the stock solution, letting it dry, and then adding a second 1 µl drop. Optical measurements were taken through the back of the coverslip to ensure that regions coupled to gold nanoparticles were directly probed.

A confocal microscope with a 100× objective was used to raster scan 10 µm by 10 µm regions of the samples. The same region was scanned first with a 405 nm CW laser to measure SSPL, then with a 532 nm CW laser to probe ASPL. During each scan 1225 individual spectra were taken. Each spectrum was then used as a data point for further statistical analysis. The major findings are summarized in Table 1. A representative ASPL spectrum is plotted against the sample's absorption and SSPL in Figure S2.

From the control sample, it can be seen that the ASPL is red-shifted and broadened in comparison with the SSPL taken over the same region (Table 1 and Figure S2). This red-shift has been observed before and has been previously attributed to an ensemble effect, as single particle measurements show identical ASPL and SSPL [5]. In this case, there may be energy transfer between closely spaced particles, with emission occurring from the lowest-energy emitting state available in a region. With low Au nanoparticle coverage, two major changes in the ASPL behavior are identified. First, the average full width at half maximum (FWHM) of both the SSPL and ASPL decreases. Second, the ASPL blue-shifts by an average of 7.2 meV in comparison with the control sample. This blue-shift is significant because it indicates that each emitted photon scavenges more thermal energy. With uniform Au nanoparticle coverage, the trend in average ASPL position and FWHM continues monotonically with a decrease in the FWHM and a further blue-shift of the ASPL spectral position. In comparison with the control, the uniform Au nanoparticle coverage sample emits an additional 10.1 meV of thermal energy per up-converted photon. It is known that coupling fluorescent semiconductors to a metal decreases their fluorescent lifetime [20], and this has been additionally demonstrated for $CsPbBr_3$ with Au nanoparticles deposited on the perovskite surface [21]. One explanation of the blue-shift reported here may be that the reduction in the fluorescence lifetime prevents the energy transfer between particles that would result in red-shifted emission. In fact, we observed a monotonic decrease in the SSPL lifetime of the $CsPbBr_3$ nanoparticles with increasing Au coverage, from 3.15 ns in the control sample, to 2.44 ns with low Au coverage, and finally 2.25 ns with uniform Au coverage (Table S2).

Notably, the standard deviation in both ASPL peak position and FWHM increases in the sample with uniform Au nanoparticle coverage. This trend highlights the major difference between the two Au nanoparticle coverage regimes. At low Au nanoparticle coverage, the majority of Au nanoparticles in a region are more than 10 nm away from other gold nanoparticles and near-field optical coupling dominates the Au-perovskite interactions. The resulting decrease in fluorescent lifetime results in excitation and emission from the same perovskite particle, before energy transfer between perovskite particles takes place. With uniform densely packed Au nanoparticle coverage, very short-range optical hot spots (smaller than a few nanometers) are expected to play a more significant role, leading to the stochastic modification of the ASPL emission that is dependent on the local order of the Au nanoparticle film, as well as the large increase in the standard deviation of the SSPL position and FWHM. While the ASPL position is nearly identical to the SSPL position in the sample with uniform Au coverage, the ASPL FWHM is much larger than that of the SSPL over the same region of the sample. This suggests that the phonon-mediated upconversion may emit from a different distribution of states than those accessible through above band gap excitation.

It is interesting to note that the LO phonon of $CsPbBr_3$ has an energy of approximately 20 meV [22], which is less than the thermal energy emitted per photon, even in the control sample. As such, each up-converted photon is scavenging the thermal energy of multiple phonons. This is especially remarkable when compared to other semiconductor materials studied for optical cooling applications which have larger LO phonon energies but only emit a single phonon worth of thermal energy with every

Table 1: Average position, full width at half maximum, and average thermal energy scavenged by each up-converted photon.

	SSPL position (nm)	ASPL position (nm)	SSPL FWHM (meV)	ASPL FWHM (meV)	Scavenged energy (meV)
Control sample	512.88 ± 1.00	514.39 ± 0.82	63.3 ± 5.0	72.8 ± 1.4	79.8
Low Au coverage	512.38 ± 2.62	512.86 ± 0.45	56.5 ± 9.8	70.96 ± 2.7	87.0
Uniform Au coverage	512.63 ± 3.33	512.24 ± 2.72	47.4 ± 16.1	70.5 ± 4.9	89.9

up-converted photon [23]. The 10 meV blue shift of the ASPL demonstrated with uniform Au coverage represents an additional half phonon of thermal energy extracted per photon.

Using the relationship $PL \propto I^b$, where *PL* is the ASPL intensity and *I* is the excitation power density, a loglog plot of laser fluence versus integrated ASPL counts may be used to extract *b*, which gives information about the excitation process. For an ideal one-photon process, every absorbed photon produces an emitted photon, and *b* is expected to be 1. However, a number of interactions, such as particle charging, may lead to *b* with a value less than 1. As with FWHM and ASPL spectral position, the standard deviation of this power law slope increases dramatically with uniform Au nanoparticle coverage, as shown in Figure 2A which plots ASPL integrated counts versus power law slope as a scatter plot, with each point corresponding to a diffraction limited region on the sample. This spread in the power dependence of the ASPL intensity is not present with low Au nanoparticle coverage, suggesting stochastic short-range interactions with the Au nanoparticles are modifying the intrinsic ASPL mechanism.

As is additionally demonstrated in Figure 2A, the raw counts of ASPL are decreased to approximately one third of the control value for the sample with low Au nanoparticle coverage. The average ASPL counts are further decreased in the sample with uniform coverage; however, the standard deviation is greatly increased. It is important to note that plasmonic substrates are known to quench PL from semiconductors that are within 4–5 nm of the metal surface, so this decrease in ASPL is not unexpected [24]. If, however, the ASPL counts are normalized to the SSPL counts from the same region, a different trend emerges. When normalized to SSPL intensity, the relative ASPL is observed to decrease with low Au nanoparticle coverage but increase with uniform coverage, as shown in Figure 2B. Here, the relative ASPL intensity is the integrated ASPL counts divided by the integrated SSPL counts for each region and normalized so that the value 1 is equal to the average intensity of the control. The scavenged energy per photon is the thermal energy required to up-convert a photon with 2.33 eV of energy (532 nm excitation source) to the spectral center of the ASPL. This plot clearly demonstrates the average blue-shift of the ASPL with increasing amounts of Au, as well as the increase in ASPL relative to its respective SSPL.

In order to estimate the plasmonic enhancement of ASPL thermal scavenging for each sample, we multiplied the relative ASPL intensity, as shown in Figure 2B, by the scavenged energy per photon. Essentially, this approximates each count as a single emitted photon with energy equal to the ASPL spectral center. An example of this is shown visually in Figure 3, where the color indicates the thermal energy scavenged at each point relative to the thermal energy scavenged, on average, by the control sample. The samples with Au nanoparticles scavenge 6.72 and 0.97 times the thermal energy that the control sample scavenges, for the high and low Au nanoparticle coverage samples, respectively. While the high coverage sample shows an impressive enhancement of thermal scavenging, the low coverage sample shows the utility of the blue-shifted ASPL. The 7.2 meV blue-shift almost entirely makes up for the 15% decrease in relative ASPL intensity. It is

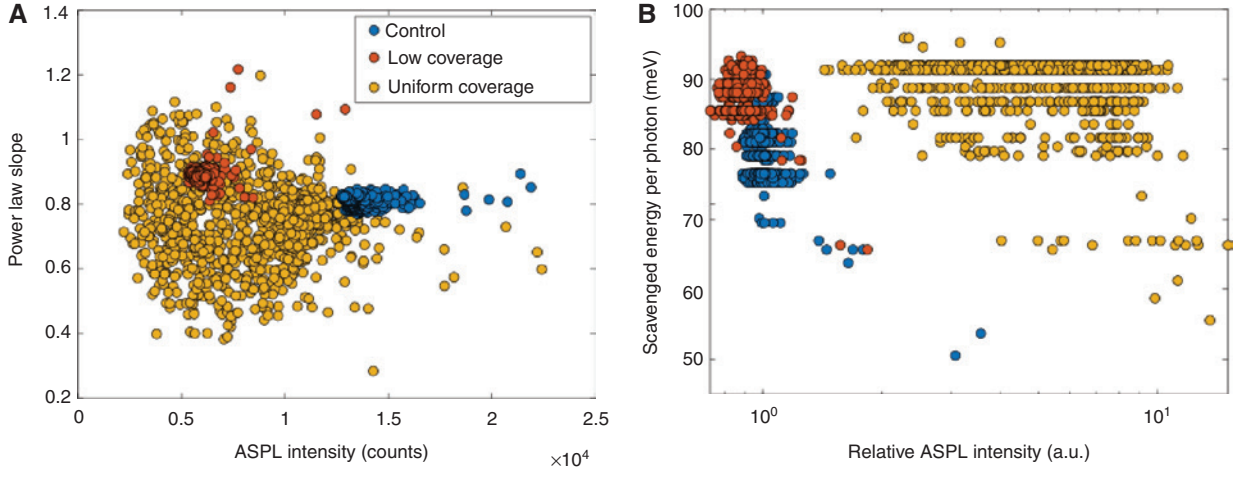

Figure 2: Modification of ASPL by plasmonic substrate.
(A) ASPL intensity versus the power law slope of the ASPL excitation power dependence. (B) ASPL intensity normalized to the SSPL intensity in the same region plotted against the average scavenged thermal energy per photon emitted. The relative ASPL intensity is scaled so that a value of 1 corresponds to the average value for the control.

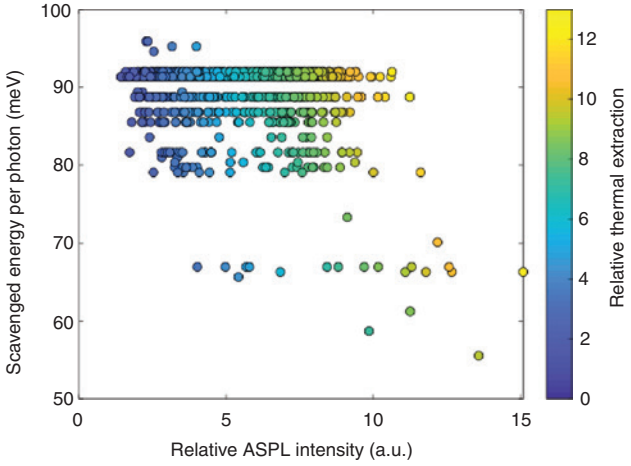

Figure 3: Relative ASPL intensity versus scavenged thermal energy per emitted photon for the sample with uniform Au nanoparticle coverage. The color of each point corresponds to the scavenged thermal energy per photon multiplied by the relative ASPL intensity and normalized to the average corresponding value for the control.

important to note that these samples are not optimized for integration into a cooling device. The absolute amount of SSPL and ASPL observed decreases with increasing Au coverage due to the photoluminescent quenching that is expected to occur when a semiconductor is in close proximity to a metal nanostructure, as well as the Au nanoparticles acting as scattering centers and promoting reabsorption losses. However, these effects should contribute similarly to the decrease in both ASPL and SSPL. As such, by normalizing ASPL to the SSPL measured over the same region, the quenching effects should be removed from the final estimate of thermal scavenging.

To verify that this 6.7-fold enhancement is in line with what could be expected given the Au nanoparticles' plasmon, we performed a full-wave optical simulation finite-difference time-domain method (FDTD) of a 40 nm in diameter Au nanoparticle embedded in a medium with a refractive index of 2.25, i.e. the refractive index of the $CsPbBr_3$ nanoparticles [25]. When illuminated with a 532 nm plane wave, the Au nanoparticle shows a 6.5 times field enhancement near its outer surface (Figure S4). While the entirety of the improvement of thermal scavenging cannot be attributed to this effect, this simulation does show that the change in thermal scavenging potential reported here is not unreasonable given the field enhancement produced by the gold nanoparticles under these conditions.

In conclusion, we have discussed the enhancement of $CsPbBr_3$ nanoparticle ASPL through coupling to a substrate with varying amounts of plasmonically active Au nanoparticles. This enhancement is due to two major effects: a blue-shift in the ASPL spectral center and an increase in the ASPL intensity relative to the SSPL intensity of the sample. The former phenomenon is likely attributable to a decrease in the fluorescent lifetime when a nanoparticle is coupled to a plasmonically active substrate. The latter phenomenon, however, is only present with high Au nanoparticle coverage of the substrate and may be analogous to the order of magnitude increase of Raman scattering demonstrated in SERS. Both effects together lead to a 6.7-fold increase in relative thermal extraction by the sample with the highest Au nanoparticle coverage. This enhancement is especially promising for applications in optoelectronic devices, where the fluorescent quenching of the $CsPbBr_3$ nanoparticles may be managed with more sophisticated photonic design while still maintaining the enhancement of the ASPL thermal scavenging.

3 Materials and methods

3.1 Chemicals

Cesium carbonate (Cs_2CO_3, Alpha Aesar, Haverhill, MA, USA, 99.995% trace metals basis), lead (II) bromide ($PbBr_2$, Alfa Aesar, 98+%), oleylamine (OAm, Sigma Aldrich, St. Louis, MO, USA, technical grade 70%), oleic acid (OA, Sigma Aldrich, technical grade 90%), 1-octadecene (ODE, Sigma Aldrich, technical grade 90%), hexanes (Sigma Aldrich, anhydrous mixture of isomers, 99%), gold nanoparticles (Sigma Aldrich, 40 nm diameter, OD 1, aqueous suspension in 0.1 mM PBS), hydrochloric acid (HCl, Macron Fine Chemicals, Center Valley, PA, USA, 36.5%–38%), and methanol (MeOH, Millipore Sigma, Burlington, MA, USA).

3.2 Preparation of Samples

$CsPbBr_3$ nanoparticles were prepared following the procedure established by Protesescu et al. [26]. In short, 0.200 g Cs_2CO_3, 0.624 ml OA, and 10 ml ODE were added to a 25-ml three-neck flask and heated at 100°C under argon flow until the Cs_2CO_3 had entirely dissolved to form Cs-oleate. In a separate 25-ml three-neck flask, 0.069 g $PbBr_2$ and 5 ml ODE were dried at 120°C under vacuum for 1 h. The solution was then placed under argon, and 0.5 ml of dried OAm and 0.5 ml of dried OA were injected to solubilize the $PbBr_2$. The temperature was increased to 180°C, and 0.4 ml of the Cs-oleate solution was swiftly injected. After 3 s, the solution was cooled with an ice bath. The final crude solution was centrifuged at 3000 g-forces for 5 min, and the supernatant was discarded. The precipitate was cleaned three times using a combination of ODE and hexane.

Initial characterization included UV-Vis and PL, as well as transmission electron microscopy (TEM), and are available in the Supplementary Information. UV-Vis spectra from 300 to 800 nm were collected on an Ocean Optics (Winter Park, FL, USA) Flame-S-UV-Vis spectrometer with an Ocean Optics DH-200-Bal deuterium and halogen light source. TEM images were collected on an FEI (Hillsboro, OR, USA) Tecnai G2 F20 ST FETEM microscope, operating at 200kV. The $CsPbBr_3$ nanoparticles are cuboids with edge lengths of 10.27 ± 0.18 nm, as determined by analyzing 60 particles using ImageJ (NIH, Bethesda, MD, USA) (Figure S1) [27].

The substrates were initially cleaned by sonicating in methanol for 1 h. The substrates with gold were placed in a vial with 1.5 ml nanopore water, 60 µl of 0.1 M HCl, and an amount of the aqueous gold nanoparticles, and then the vial was centrifuged for 1 h at 3000 *g*-forces. The substrate was then rinsed with hexane before depositing perovskites. To each substrate, 1 µl of the stock $CsPbBr_3$ solution was drop-cast and allowed to dry, and then another 1 µl was added. All optical measurements were taken through the cover slip to ensure that regions of $CsPbBr_3$ coupled to gold nanoparticles were being probed.

3.3 Analysis of ASPL

All measurements of up-conversion were taken using a WITec (Ulm, Germany) alpha 300 RA confocal microscope with an EC Epiplan-NEOFLUAR (ZEISS, Oberkochen, Germany) 100× objective with a 0.9 numeric aperture. Measurements were taken at room temperature as a series of spectra, using a piezoelectric stage to raster scan an area of the sample. Each measurement was taken over a 10 µm by 10 µm area as a series of 35 lines of 35 spectra. ASPL was measured using a 532 nm Nd:YAG CW laser (WITec, Ulm, Germany). SSPL was measured using a 405 nm diode CW laser (RGBLase LLC, Fremont, CA, USA). ASPL spectra were collected with an excitation fluence of 2000 W/cm^2. SSPL spectra were collected with an excitation fluence of 1000 W/cm^2. The power dependence of the ASPL was determined using a range of laser fluences from 2000 to 50,000 W/cm^2. Each spectrum was processed using WITec's Project FOUR software to remove cosmic rays before further analysis.

3.4 Simulation of Au nanoparticle field enhancement

The simulation was run using a commercially available FDTD solver (Lumerical, Vancouver, BC, Canada). A 40 nm diameter gold nanoparticle with refractive index as measured by Johnson and Christy [28] was simulated in a medium with refractive index of 2.25 as an approximation of the $CsPbBr_3$ nanoparticles surrounding the Au nanoparticles [25]. The gold nanoparticle was illuminated with a plane wave source at 532 nm in a simulation area using perfectly matched layer boundary conditions.

3.5 Measurement of SSPL lifetime

Fluorescence lifetime was measured using an Olympus (Center Valley, PA, USA) FV 1000 confocal platform with a PicoQuant (Berlin, Germany) TCSPC FLIM add-on. Samples were excited using a 405 nm pulsed laser. Data was fit to a biexponential decay using PicoQuant's SymPhoTime 64 software suite.

4 Supplementary Information

Supplementary material is available online on the journal's website or from the author. The supplementary information included initial characterization of $CsPbBr_3$ and Au nanoparticles, as well as statistical analysis of the power law fits.

Acknowledgments: This work was supported by the Air Force Office of Scientific Research under award number FA9550-16-1-0154. M.S. also acknowledges support from the Welch Foundation (A-1886). Use of the Texas A&M University Laboratory for Synthetic-Biologic Interactions and Mr. Justin Smolen are acknowledged. We also acknowledge Nicki Hogan for help with optical simulations.

References

[1] Duan C, Liang L, Li L, Zhang R, Xu ZP. Recent progress in upconversion luminescence nanomaterials for biomedical applications. J Mater Chem B 2018;6:192–209.
[2] Wen S, Zhou J, Zheng K, Bednarkiewicz A, Liu X, Jin D. Advances in highly doped upconversion nanoparticles. Nat Commun 2018;9:2415.
[3] Ha ST, Shen C, Zhang J, Xiong Q. Laser cooling of organic-inorganic lead halide perovskites. Nat Photonics 2016;10:115–21.
[4] Morozov YV, Draguta S, Zhang S, et al. Defect-mediated CdS nanobelt photoluminescence up-conversion. J Phys Chem C 2017;121:16607–16.
[5] Morozov YV, Zhang S, Brennan MC, Janko B, Kuno M. Photoluminescence up-conversion in CsPbBr 3 nanocrystals. ACS Energy Lett 2017;2:2514–5.

[6] Rakovich YP, Donegan JF, Vasilevskiy MI, Rogach AL. Anti-Stokes cooling in semiconductor nanocrystal quantum dots: a feasibility study. Phys Status Solidi 2009;206:2497–509.
[7] Roman BJ, Sheldon M. The role of mid-gap states in all-inorganic $CsPbBr_3$ nanoparticle one photon up-conversion. Chem Commun 2018;54:6851–4.
[8] Seletskiy DV, Epstein R, Sheik-Bahae M. Laser cooling in solids: advances and prospects. Reports Prog Phys 2016;79:096401.
[9] Sheik-Bahae M, Epstein R. Optical refrigeration. Nat Photonics 2007;1:693–9.
[10] Sheik-Bahae M, Epstein RI. Can laser light cool semiconductors? Phys Rev Lett 2004;92:247403.
[11] Zhang J, Li D, Chen R, Xiong Q. Laser cooling of a semiconductor by 40 kelvin. Nature 2013;493:504–8.
[12] Akizuki N, Aota S, Mouri S, Matsuda K, Miyauchi Y. Efficient near-infrared up-conversion photoluminescence in carbon nanotubes. Nat Commun 2015;6:1–6.
[13] Ignatiev IV, Kozin IE, Ren HW, Sugou S, Masumoto Y. Anti-Stokes photoluminescence of InP self-assembled quantum dots in the presence of electric current. Phys Rev B 1999;60:1–4.
[14] Rakovich YP, Filonovich SA, Gomes MJM, et al. Anti-Stokes photoluminescence in II-VI colloidal nanocrystals. Phys Status Solidi Basic Res 2002;229:449–52.
[15] Wang X, Yu W, Zhang J, Aldana J, Peng X, Xiao M. Photoluminescence upconversion in colloidal CdTe quantum dots. Phys Rev B – Condens Matter Mater Phys 2003;68:1–6.
[16] Ye S, Zhao M, Yu M, et al. Mechanistic investigation of upconversion photoluminescence in all-inorganic perovskite $CsPbBrI_2$ nanocrystals. J Phys Chem C 2018;122:3152–6.
[17] Koscher BA, Swabeck JK, Bronstein ND, Alivisatos AP. Essentially trap-free $CsPbBr_3$ colloidal nanocrystals by postsynthetic thiocyanate surface treatment. J Am Chem Soc 2017;139:6566–9.
[18] Kang J, Wang LW. High defect tolerance in lead halide perovskite $CsPbBr_3$. J Phys Chem Lett 2017;8:489–93.
[19] Yamamoto YS, Ozaki Y, Itoh T. Recent progress and frontiers in the electromagnetic mechanism of surface-enhanced Raman scattering. J Photochem Photobiol C Photochem Rev 2014;21:81–104.
[20] Hartsfield T, Gegg M, Su PH, et al. Semiconductor quantum dot lifetime near an atomically smooth Ag film exhibits a narrow distribution. ACS Photonics 2016;3:1085–9.
[21] Roman BJ, Otto J, Galik C, Downing R, Sheldon M. Au exchange or Au deposition: dual reaction pathways in Au-$CsPbBr_3$ heterostructure nanoparticles. Nano Lett 2017;17:5561–6.
[22] Iaru CM, Geuchies JJ, Koenraad PM, Vanmaekelbergh D, Silov AY. Strong carrier-phonon coupling in lead halide perovskite nanocrystals. ACS Nano 2017;11:11024–30.
[23] Sun G, Chen R, Ding YJ, Khurgin JB. Upconversion due to optical-phonon-assisted anti-stokes photoluminescence in bulk GaN. ACS Photonics 2015;2:628–32.
[24] Kim D, Yokota H, Taniguchi T, Nakayama M. Precise control of photoluminescence enhancement and quenching of semiconductor quantum dots using localized surface plasmons in metal nanoparticles. J Appl Phys 2013;114:154307.
[25] Dirin DN, Cherniukh I, Yakunin S, Shynkarenko Y, Kovalenko MV. Solution-grown $CsPbBr_3$ perovskite single crystals for photon detection. Chem Mater 2016;28:8470–4.
[26] Protesescu L, Yakunin S, Bodnarchuk MI, et al. Nanocrystals of cesium lead halide perovskites (CsPbX3, X=Cl, Br, and I): novel optoelectronic materials showing bright emission with wide color gamut. Nano Lett 2015;15:3692–6.
[27] Abramoff MD, Magalhães PJ, Ram SJ. Image processing with ImageJ. Biophotonics Int 2004;11:36–42.
[28] Johnson PB, Christy RW. Optical constants of the noble metas. Phys Rev B 1972;6:4370–9.

Supplementary Material: The online version of this article offers supplementary material (https://doi.org/10.1515/nanoph-2018-0196).